Catalysis Today 282 (2017) 204–213

Contents lists available at ScienceDirect

Catalysis Today

journal homepage: www.elsevier.com/locate/cattod

# Effect of the support and promoters in Fischer-Tropsch synthesis using supported Fe catalysts

L.A. Cano[a,*], A.A. Garcia Blanco[b], G. Lener[b], S.G. Marchetti[a], K. Sapag[b]

[a] Facultad Ciencias Exactas – Universidad Nacional de La Plata, Argentina
[b] INFAP – Universidad Nacional de San Luis, Argentina

ARTICLE INFO

*Article history:*
Received 22 February 2016
Received in revised form 23 June 2016
Accepted 28 June 2016
Available online 4 July 2016

*Keywords:*
Fischer Tropsch
Supported Fe
Potassium
Copper

ABSTRACT

The effect of support and promoters on the catalytic properties of Fe supported in the FTS was studied. Precursors of supported Fe on $SiO_2$ and SBA −15 were synthesized and doped with Cu and K. The precursors were activated in pure $H_2$ and catalytically tested with a mixture of $H_2$:CO = 2:1, T = 543 K and P = 10 bar. The samples were characterized by atomic absorption, $N_2$ adsorption, X-ray diffraction, TEM and TPR. Also, we used the DFT to study the changes of the electronic structure when the Fe, K and Cu are adsorbed on the SBA-15 surface. The incorporation of different ions do not alter the structural and textural properties of the support. In the FTS, all the catalysts supported on SBA-15 presented a low selectivity towards methane and a promising hydrocarbon production in the range of gasoline, showing positive effect of the support for iron catalysts for the FTS reaction. The activity order obtained was: Fe/K-SBA-15 > Fe/Cu-SBA–15 ≈ Fe-SBA–15 > Fe-$SiO_2$, which is the same order for the selectivity towards olefins. The presence of K on the SBA-15 surface increases the activity and selectivity towards olefins; an effect that can be attributed to the electrostatic effect generated by the alkaline ions.



## 1. Introduction

The Fischer Tropsch Synthesis (FTS) allows to obtain hydrocarbons (HC) from syngas (a mixture of CO: $H_2$) and has been extensively studied for more than fifty years. Since its discovery, the interest in FTS has followed the fluctuations in the value of crude oil and the knowledge of the existence of reserves [1]. In recent years an increase in research in this subject will note, which shows a renewed interest in the FTS. The problems associated with current oil extraction and processing technologies, more stringent environmental regulations and the need for new investments in the refinery sector, are making FTS (or, in a broader sense, the process of converting gas to liquids) more attractive and viable for the production of hydrocarbons. Therefore, further efforts to increase basic and applied knowledge on the subject appears to be attractive.

Different metals are active as catalysts in the FTS, but today, Co and Fe are the only reasonable commercial catalysts for this process [2]. When iron is used as catalyst, the FTS occurs simultaneously with the water–gas shift (WGS) reaction. It consumes CO and water obtained from the FTS and produces additional $H_2$ and $CO_2$. For this reason, the iron catalysts are the best choice when a syngas poor in hydrogen is used. This situation occurs if the syngas is produced by gasification of coal or biomass. Besides, the iron catalysts are preferred to cobalt catalysts, since they have lower cost, lower methane selectivity, lower sensitivity to poisons, and higher flexibility to lead the selectivity to alkenes, oxygenates, or branched hydrocarbons according to the promoters or the operative variables used.

Alkali metals have been widely studied as promoters to increase the activity and selectivity to olefins in the FTS when iron bulk catalysts are used. The most used are alkali metals of the first group of the periodic table, and among them potassium (K) has been considered it provides the best cost-benefit ratio compared with other alkali metals of the group. Apparently potassium increases the adsorption of CO and consequently decreases the relative amount of adsorbed hydrogen. From this point of view, potassium decreases the hydrogenation of secondary alkenes. One possible explanation is that potassium donates electrons to iron and facilitates the dissociation of CO, which tends to accept electrons from it [3,4]. The role of potassium in the increased formation of heavy hydrocarbons was recently investigated by Ribeiro [5] using TPR-EXAFS/XANES-TPR experiments. There is shown a possible electronic effect by a systematic increase in the speed of carburization catalysts Fe: Si: alkali as a function of increasing basicity promoter. With accordance with this work, Li [6] concluded that potassium promotes the formation of new active sites during the

* Corresponding author.
*E-mail address:* lcano@quimica.unlp.edu.ar (L.A. Cano).

http://dx.doi.org/10.1016/j.cattod.2016.06.054
0920-5861/

subsequent carburization and reduction of iron oxides to facilitate rapid formation of nucleation sites to generate small crystallites of iron carbides.

It is well known that copper can facilitate the reduction at low temperature and improve the formation of FTS active phase [7–11]. Cu is thus often used to improve the catalyst performance and offset disadvantages of structure promoters for Fe-based catalysts. Although the function of copper in facilitating catalyst reduction has been widely accepted, its influence on FTS product distribution has not been well addressed. Wachs [12] and O'Brien [11] observed that copper had no effect on product selectivity; this was established by conducting the FTS reaction in both differential fixed-bed and slurry-phase reactors. Bukur [13] reported that incorporating Cu into iron-based catalysts resulted in an increase in the average molecular weight of hydrocarbon products; however, Li [8] reported high $CH_4$ selectivity on a Cu-promoted Fe–Zn catalyst.

Apart from detailed studies on the effects of the Cu promoter on catalyst reduction and FTS properties, the exact role and physicochemical state of the Cu species in promoted catalysts has rarely been studied. Wielers [14,15] investigated hydrogen activated silica supported bimetallic Fe–Cu catalysts using Mössbauer and IR spectroscopies. They reported that the Cu phase facilitated the reduction of $Fe^{3+}$ species to $Fe^{2+}$ (iron (II) silicate) species and, subsequently to zero-valent Fe. The zero-valent Fe was present as monometallic Fe particles as well as bimetallic Fe–Cu species. In an X-ray photoelectron spectroscopy (XPS) study, Wachs et al. [12] characterized the surface of a pre-reduced, passivated FTS catalyst after in situ re-activation in $H_2$ and observed agglomeration of the Cu phase on the surface of the reduced catalysts (i.e., decreasing Cu/Fe ratios). De Smit et al. [16] investigated the structural properties of unsupported ($Fe_2O_3$ and $Fe_2O_3$-Cu) and supported ($Fe_2O_3$-Cu-KSi) catalysts during pretreatment ($H_2$ and syngas) and FTS at 1 bar by using combined X-ray absorption fine structure spectroscopy (XAFS) and wide angle X-ray scattering (WAXS) techniques. They reported that Cu significantly increased the reduction rate of the catalysts to zero-valent Fe species and increased the FTS activity and selectivity toward longer hydrocarbon products.

Although a large number of studies were carried out on the influence of copper on FTS selectivity, controversy persists, because these studies were conducted under different conditions or over different catalytic systems. Therefore, further investigation is needed to illustrate the intrinsic relationship between Cu promoter and the FTS selectivity.

The development of supported Fe catalysts of high activity is attractive as it would allow its use in the most economical reactors, such as "slurry", avoiding the high attrition rate experienced by mass Fe catalysts. On the other hand, it would be possible to increase the selectivity of the synthesis by controlling the crystal size of the active phase. This method is based on the fact that in some heterogeneous catalytic reactions, the activity of the solid is a function of the crystal size of the active phase, generally in the 1–10 nm range. These reactions are known as "structure sensitive" [17]. In the literature, there is some early evidence that the FTS is "structure sensitive" [18], and more recently, this property was confirmed by using supported Co and Fe catalysts [19–22]. Today, the concept of "structure sensitive" involves the activity and selectivity of the catalyst. This idea was recently verified by Bezemer [22] using Co particles with sizes between 2.6 and 27 nm supported on carbon nanofibers. These authors found that when the cobalt particle size was reduced from 16 to 2.6 nm, the turnover frequency for CO hydrogenation decreased about twenty times, while $C^{5+}$ selectivity decreased from 85 to 51 wt.%. Therefore, it would be possible to achieve an improvement in the catalyst selectivity if particles of supported Fe oxides, with a determined average diameter and a narrow size distribution, were obtained. In order to get this scope, an "inert" support with a narrow pore-size distribution and thermal stability would be selected. Besides, the pore diameters of the support must be large enough to locate the iron oxide crystals inside the pores, avoiding their migration to the outer surface during the activation steps. The mesoporous solid named SBA-15 seems to fulfill the above conditions since it has a narrow pore-size distribution, with a hexagonal arrangement, whose diameters can be varied between 5 and 30 nm, wall thickness between 3 and 6 nm, and specific surface area between 700 and 1000 $m^2/g$ [23,24]. The use of this type of support is not enough to obtain a narrow crystal-size distribution in the desired size range of the active Fe species. In order to get this scope, it is necessary to introduce the total iron loading inside the support channels avoiding its migration to the outer surface when the catalyst is "working" since the controlling effect on the sintering process would be lost. Achieving these objectives represents a real challenge.

Another important aspect is to investigate how the electronic density of the active site changes in the presence of promoters. The density functional theory (DFT) is an important method to get optimized local structures, and allows the study of the electronic structure and its change, as well as the distribution of the electronic density of the metal/support interface, which function as active site in a catalytic process. In this context, Park et al. use DFT to investigate the flux of electronic density in the adsorbed state of the K atoms doped Fe surfaces applied to FT process [25].

In the bibliography the information of DFT study of the effect of promoters in the electronics structure of the metallic site and their interface with SBA-15 has not been explored. In this work we reported experimental results of the effect of K and Cu promoters in Fe-SBA-15 materials and it is complemented with DFT calculations to investigate how change the electronic density due of the presence of the K and Cu promoters in Fe-SBA-15 catalyst.

## 2. Material and methods

### 2.1. Catalyst preparation

The SBA-15 support was synthesized according to the methodology proposed by Zhao et al. [23,24] using Pluronic triblock copolymer P123 (EO20-PO70-EO20) as organic structure-directing agent and tetraethyl orthosilicate (TEOS) as silica source. Thus, 12 g of Pluronic P123 was dissolved in 360 ml of water and 60 ml of HCl solution (37%, w/w) with stirring at 313 K for 3 h. Then, 27 ml of TEOS was added, and the solution was kept stirring at 313 K for 24 h. The mixture was aged at 363 K overnight, without stirring. The solid was recovered by filtration, washed, and dried in air at room temperature (RT). Calcination in air was carried out at 773 K during 6 h at 1 K/min. To determine the effect of the support, a commercial silica (Silica gel, Grade 10184, pore size 100 Å, 70–230 mesh, Sigma Aldrich) was used to compare with the SBA-15. The two supports were impregnated by the incipient wetness impregnation method with $Fe(NO_3)_3{\cdot}9H_2O$ ethanolic solution to produce a nominal Fe loading of 10% w/w in a single step. The solids were dried using a rotary evaporator at 313 K for 24 h and finally calcined in a flow of NO (1% v/v)/He (100 $cm^3$/min) from RT to 723 K at a heating rate of 1 K/min and kept at this temperature for 4 h. The samples thus obtained were called Fe-SBA-15 and Fe-$SiO_2$.

To analyze the effect of Potassium and Cupper as promoters of Iron, SBA-15 support was impregnated with two different ethanolic solutions: a mix of $Fe(NO_3)_3{\cdot}9H_2O$ and $Cu(NO_3)_2.2{,}5H_2O$ in ethanolic solution to produce a nominal loading of 10% w/w to Iron and 0,05% w/w to Cu and another one with a mix of $Fe(NO_3)_3{\cdot}9H_2O$ and $KNO_3$ in ethanolic solution to produce a nominal loading of 10% w/w of Iron and 0,1% w/w of Potassium. The solids were dried and calcined as mentioned above and were called Fe/K-SBA-15 and Fe/Cu-SBA-15.

The Potassium and Cupper content were adopted as the basis of the atomic ratio of Fe/K and Fe/Cu possessed by bulk catalysts used in the Fischer-Tropsch industry mentioned in some publications [9,16,26].

### 2.2. Catalyst characterization

The samples were characterized by atomic absorption spectroscopy (AAS), Low Angle – X-ray diffraction (LA XRD) at low angles, $N_2$ adsorption (BET), transmission electron microscopy (TEM), temperature-programmed reduction (TPR) and density functional theory (DFT).

The Fe content of the solid was determined by atomic absorption on an AA/AE Spectrophotometer 457 of Laboratory Instrumentation Inc. The sample was digested in a mixture of HCl and HF up to complete dissolution and then was treated according to conventional methods for this technique.

The X-ray diffraction patterns at low angles were recorded in a Shimadzu equipment, XD3A model, using Cu Kα radiation generated at 40 kV and 40 mA in the range 2&z.Theta; = 0.5–9° with steps of 0.02° and counting time of 2 s/step.

The adsorption-desorption isotherms of $N_2$ at 77 K were measured in Quantachrome, Autosorb 1-MP equipment. The samples were previously outgassed at 250° C for 12 h. Textural properties, such as the specific surface area ($S_g$), micropore volume ($V_{\mu p}$), total pore volume ($V_{TP}$), and pore width ($W_p$) were calculated from the experimental data. $S_g$ and $V_{\mu p}$ were obtained using the BET and the $\alpha_s$-plot methods, respectively. The $W_p$ was calculated by means of the VBS method, which is described in [27].

The transmission electron microscopy micrographs were taken using a microscope JEOL model JEM-1200 EX II. The sample was previously incorporated into a Aradilta resin and was subsequently cut with an ultramicrotome Sorvall MT 5000.

The temperature programmed reduction experiments were performed on a Micromeritics equipment (Chemisorb 2705) overflow of a mixture of $H_2$ and $N_2$ containing 5% of $H_2$ at 30 $cm^3$/sec. The sample was heated from 20 to 1000 °C with a rate of 10°/min.

#### 2.2.1. Computational method of density functional theory

For the Density functional theory (DFT) calculations we have used the generalized gradient approximation (GGA) in the version of Perdew–Burke–Ernzerhof (PBE) [28] implemented in the SIESTA code [29]. It uses Troullier–Martins norm-conserving pseudopotentials [30] to represent the nucleus and core electrons of the considered species. The basis set used for the expansion of the Kohn–Sham eigenstates is composed of a set of numerical atomic orbitals including polarization orbitals. An energy shift of 50 meV has been chosen as a compromise between accuracy and computational efficiency. We have taken an energy cutoff of 200 Ry and a double-ζ plus polarization orbital basis set (DZP). All geometries have been optimized until the force on each atom was less than 0.01 eV/Å. We use $3 \times 3 \times 3$ and $3 \times 3 \times 1$ k-point for the Brillouin zone (BZ) for the bulk and slab representation respectively.

The surface of the mesoporous SBA-15 material was represented by the β-cristobalite structure (ICSD # 77459) [31]. In order to investigate the metal adsorption properties, the 001 face of β-cristobalite was used and one slab of 8 layers of the $SiO_2$, where the last two layers were fixed in the optimization. In order to represent the chemistry of the surface of SBA-15 some SiOH terminal silanols were displayed on the surface [32]. In order to achieve the different optimized structures, firstly the β-cristobalite bulk was optimized with variable cell condition. Secondly, it was generated, and latter the 001 surface was relaxed extending the z axes to 20 Å. Finally, different atomic species were placed on the surface and relaxed. The adsorption energy, the differential of electronic density and the band gap energy, among others properties were calculated thereof.

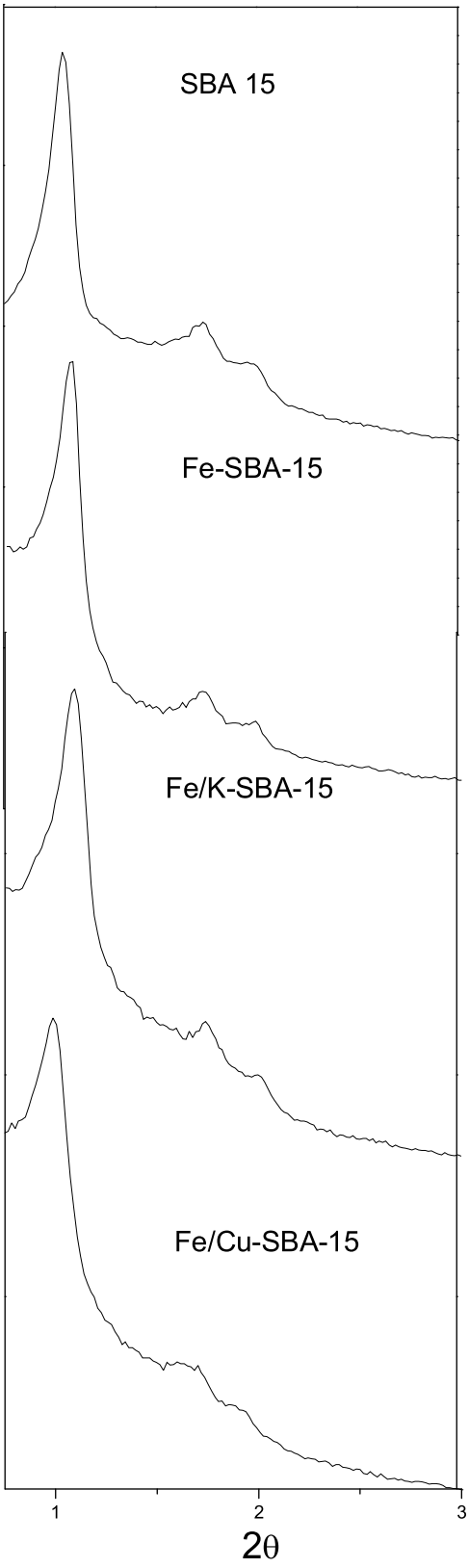


**Fig. 1.** Xrd patterns for SBA-15 and Fe-SBA-15 materials.

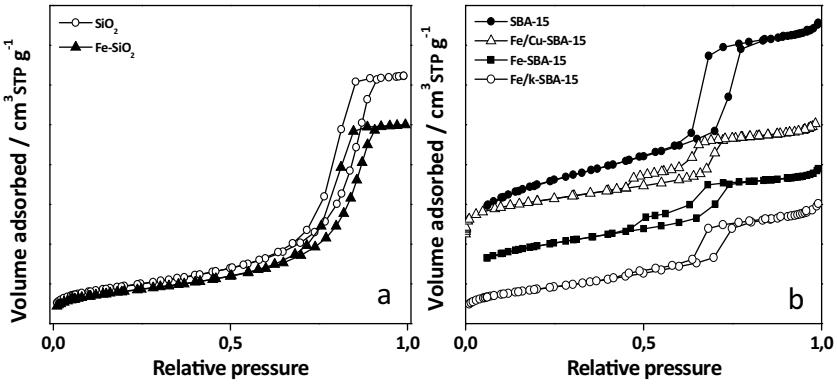


**Fig. 2.** $N_2$ adsorption-desorption isotherms at 77 K for the supports and the catalysts.
a: $SiO_2$ and Fe-$SiO_2$, b: SBA-15 and Fe-SBA-15 materials. The adsorption isotherms of the SBA-15 and SBA-15 supported catalysts have been displaced in the y axis, in order to show their shape cleary.

**Table 1**
Textural properties of the supports and the catalysts and metal loading of the catalysts.

| Material | $S_g$ ($m^2\ g^{-1}$) | $V_{\mu P}$ ($cm^3\ g^{-1}$) | $V_{TP}$ ($cm^3\ g^{-1}$) | $W_p$ (VBS) (nm) | Metal Loading (%w/w) |
|---|---|---|---|---|---|
| *SBA-15* | 899 | 0.111 | 1.0 | 8.8 | |
| *$SiO_2$* | 342 | 0 | 0.9 | 17 | |
| *Fe-$SiO_2$* | 295 | 0 | 0.77 | 16.1 | 8.7 |
| *Fe-SBA-15* | 522 | 0.05 | 0.5 | 8.1 | 8 |
| *Fe/K-SBA-15* | 314 | 0 | 0.45 | 8.3 | 8.6/0.12 |
| *Fe/Cu-SBA-15* | 390 | 0.02 | 0.47 | 6.7 | 9.1/0.05 |

The adsorption energy $E_{ads}$ can be calculated from:

$$E_{ads} = E_{system} - (E_{SBA-15} + E_{Metal}) \quad (1)$$

Where $E_{system}$ is the total energy of the system, $E_{SBA-15}$ is the slab energy of the SBA-15 relaxed and $E_{Metal}$ is the energy of Fe atom or FeX (X= K, Cu) relaxed as appropriate. The energy of the system is minimized, allowing relaxation of all atomic coordinates of the entire system while the two innermost layers remains fixed. The pseudo charge density difference $\Delta h$ is defined as [33].

$$\Delta h = \eta_{system} - (\eta_{SBA-15} + \eta_{Metal}) \quad (2)$$

where $\eta_{system}$ is the pseudo charge density of the system, $\eta_{SBA-15}$ and $\eta_{Metal}$ are the pseudo charge density of the isolated metallic or bimetallic adsorbent and SBA-15 slab, respectively. The density of states (DOS) of the system and the projection onto different individual atomic orbitals (PDOS), have also been calculated. The molecular graphics have been done with the XCRYSDEN package [34].

### 2.3. Activity and selectivity measurements

Catalytic tests were carried out in a fixed-bed micro-activity reactor (Microactivity Reference, PID Eng&Tech. S.L.). About 0.4 g of catalyst were used, with a particle size between 0.297-0.500 mm, diluted with 4 g of SiC for each experiment. The catalytic reactions were performed at 10 bar of pressure, with a ratio $H_2/CO = 2$, and a temperature of 543 K. Prior to the catalytic tests, the catalysts were reduced in situ using a flow of pure hydrogen (99.999% purity) at atmospheric pressure and 703 K for 6 h. After the reduction treatment, the temperature of the reactor was lowered up to the reaction temperature. The gaseous products of the reaction were studied on-line with a gas chromatograph using TCD and FID detectors. Waxes were collected in a trap kept at 353 K and analyzed off-line.

## 3. Results and discussion

The ordered hexagonal structure of mesoporous SBA-15, used as support, was verified by XRD (Fig. 1). The impregnation and calcination treatments, which lead to obtaining Fe-SBA-15, Fe/K-SBA-15 y Fe/Cu-SBA-15 do not change the structural properties of the mesoporous support, as was verified by XRD (Fig. 1). Iron nitrates were decomposed by calcination in a flow of NO (1% v/v)/He since it has been recently demonstrated by Sietsma and den Breejen [35,36] that calcination with NO flow produces Co particles with significantly smaller sizes in the $Co/SiO_2$ system when cobalt nitrate salt is used in the impregnation step. Besides, a significant narrowing in particle size distribution was obtained when NO flow was used instead of air flow. These results could be explained since NO is one of the nitrogen oxides produced during cobalt nitrate decomposition; therefore, if it is fed during the calcination process, the salt decomposition would occur in a controlled way and the clustering and growth of the nanoparticles would be avoided. Hence, we used iron nitrate as a precursor, in order to achieve similar results in our materials.

Comparing the values of the diffraction angles of impregnated SBA-15 with those obtained for the pure support, a slight difference in the position of the first diffraction line is observed. In the impregnated supports this line is around 0.3° above the value shown in the pure SBA-15. Bearing in mind that the position of this peak is inversely related to the interplanar spacing of the SBA-15, the increase in the angle of diffraction evidence a lower value of lattice parameter in the impregnated support [37].

In Fig. 2, are shown the $N_2$ adsorption-desorption isotherms of the supports ($SiO_2$ and SBA-15) and the catalysts. The shape of the isotherms gives a good idea of the pore structure of the materials. In Fig. 2a, we shown the isotherms of $SiO_2$ and Fe-$SiO_2$, these are characteristic of mesoporous silica, with no apparent contribution of micropores, a fact which suggested by the low adsorption at low relative pressures, while the presence of a hysteresis loop indicates the presence of mesoporosity. By analyzing the textural properties of $SiO_2$ and Fe-$SiO_2$, a decrease of $V_{TP}$ and $S_g$ in comparison with

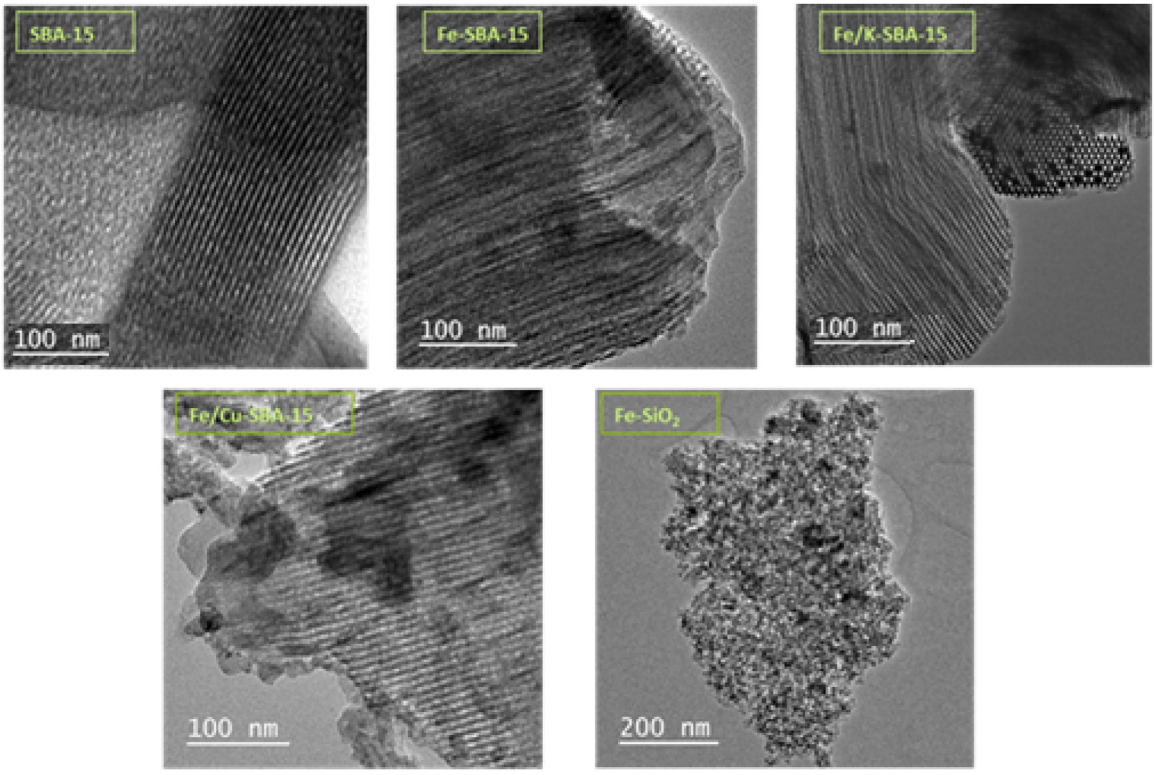


**Fig. 3.** TEM micrographs of the catalysts.

the support, without substantial changes in $W_p$, can be observed. This would imply a partial pore filling of the support with the Fe oxide species (Table 1). The Fe content in each catalysts obtained by AAS is also shown in Table 1.

In the isotherms of Fig. 2b (SBA-15 and Fe-SBA-15 materials) the shape of the isotherms is characteristic of SBA-15 materials. There is a steep increase in the adsorbed amount at low relative pressures, due to the micropores present in these materials (interconnecting the mesoporous channels) [38,39], and another one at relative pressures close to 0.6 which corresponds to the capillary condensation in the primary mesopores. The latter steep increase is characteristic of capillary condensation in pores with a specific pore size, such as the case of SBA-15. The hysteresis loop observed in the isotherm of the SBA-15 has the characteristic shape of a H1 hysteresis loop according to the IUPAC classification, which corresponds to ordered, cylindrical and independent pores [40]. However, the isotherms of the other materials (Fe-SBA-15, Fe/K-SBA-15, Fe/Cu-SBA-15) present a different hysteresis loop, characterized by the appearance of an additional low-pressure hysteresis. That kind of hysteresis has been previously reported in SBA-15 materials with pore blockage in their primary mesopores, due to the presence of nanoparticles inside those channels [41–43]. As a consequence, the appearance of that kind of hysteresis in our materials is an evidence of the presence of nanoparticles of the incorporated oxides inside the channels of the SBA-15. That hysteresis is apparently smaller in the Fe/K-SBA-15, which could be related to a minor presence of pore blockage in that sample.

The textural properties shown in Table 1, evidence a high decrease in the micropore volume in the supported catalysts with respect to the support, and additionally, an important decrease in their $S_g$ with respect to the original SBA-15 is observed. Furthermore, the value of the $W_p$ of the catalysts is similar to the one of the supports, which could again indicate a partial filling of the pores.

In Fig. 3 are shown the transmission electron micrographs of the impregnated supports. The channels of the SBA and their partial filling with metal oxides, which are the darkest areas, can be observed. In the Fe-$SiO_2$ catalyst we see a disordered structure and hence larger particles.

The best example is the catalyst of iron and potassium, where filled pores are clearly visible, this picture was taken parallel to the axis of the support channel. There can be seen the mouths of empty pores of the support (lightest part) with uniform distribution and hexagonal system and partial filling thereof with oxides of Fe (darker parts).

This micrography evidence the formation of nanometric cylinders of Fe oxides within the SBA-15 channels, as has been previously reported by our group [44].

In the case of Fe/Cu-SBA-15, the dark-grey regions are bigger that in the others catalysts, indicating a larger aggregate of Fe and Cu oxides particles.

In summary, we see that we have successfully introduced the Fe, K and Cu within the pores of the supports via alcoholic solution impregnation, maintaining the ordered structure of SBA-15 and partially filling some of its pore channels with metal oxides as has previously reported in the literature [45]. These observation are in agreement with the results obtained from gas adsorption characterization.

In Fig. 4 are shown the temperature-programmed reduction profiles of the Fe-SBA-15, Fe/K-SBA-15 and Fe/Cu-SBA-15 materials. Similar behaviors are observed in samples Fe-SBA-15 and Fe/K-SBA-15, several peaks are observed that would correspond to the reduction of $Fe^{3+}$ and $Fe^{2+}$ species, as well as to the reduction of oxides with different particle sizes and different interaction with the $SiO_2$, which reduce at different temperatures. In the Fe/K-SBA-15 a peak 1000–1100 K is observed that is not present in the Fe-SBA-15 sample, this signal can be attributed to the formation of $K^+$ ionic species on the SBA-15 surface [46].

The TPR profile of the Fe/Cu-SBA-15 shows the main reduction peak displaced towards lower temperatures. Moreover, the shoulder of the peak at 500 K could be assigned likely to the reduction

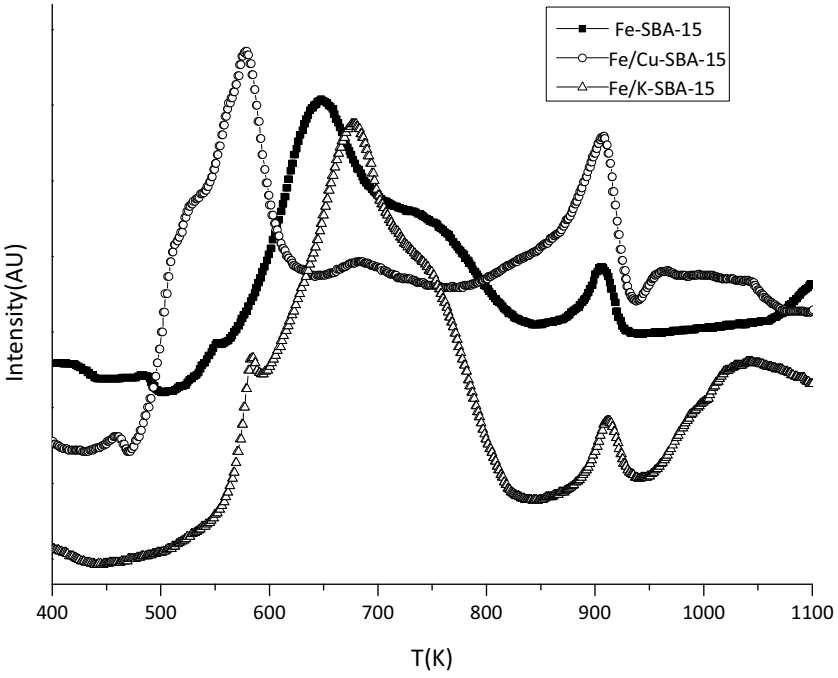


**Fig. 4.** TPR profiles of the catalysts.

**Table 2**
Adsorption energy and band gap energy of the different catalyst.

| System | $E_{ads}$ (eV) | $E_{Band\text{-}Gap}$ (eV) |
|---|---|---|
| *SBA-15* | – | 3.8 |
| *Fe-SBA-15* | −1.32 | 1.3 |
| *Fe/K-SBA-15* | −2.41 | 0 |
| *Fe/Cu-SBA-15* | −2.84 | 0 |

of small clusters of CuO on SBA-15 [46] and the main peak close to 530 K could be attributed to the reduction of a mixed oxide $FeCuO_x$ which forms a FeCu alloy, suggesting the high interaction between $Fe_2O_3$ and CuO, this effect has been reported in previous a work using $TiO_2$ as support [47]. The location of the new reduction peak is at lower temperatures than the iron species, but at higher temperatures than the usual lowest reduction temperature of CuO. This fact evidences the role of copper addition in the reduction behavior of a supported iron catalyst, and could be attributed to the formation of an alloy of CuFe.

As mentioned above, we used DFT calculations to investigate the adsorption energy and the changes in the electronic structure for the adsorptive state of iron and copper/potassium promoters on the surface of SBA-15.

Table 2 shows the adsorption energy and the band gap energy of the relaxed geometries for the different interfaces. The adsorption energy calculated for the Fe-SBA-15 system is −1.32 eV whereas it was −2.41 and −2.84 eV for Fe/K-SBA15 and Fe/Cu-SBA15 respectively. These results indicate that both bimetallic composite Fe/X-SBA-15 (X = K, Cu) present a more stable interaction with the support than Fe-SBA-15 interface.

Fig. 5 shows the final geometries of the optimization and the differential of the electronic density of the systems. Fig. 5a and b shows the top view of the surface in the Fe-SBA-15, where is shown that the Fe atom interact with the hydroxyl groups of the surface, creating a distribution of electronic density between the iron atom and the Si-OH groups close to the Fe atom site.

In the Fe/Cu-SBA-15 system, an accumulation of electronic density surrounding the copper atom is observed, where the iron atom distributes electronic density towards the surface and the copper atom (Fig. 5c-d). Besides, in the plane of the surface (Fig. 5d) it can be seen the accumulation of electronic density between the Cu atom and the hydroxyl group, and the flux of electronic density from SiO-OH-Fe to SiO-OH-Cu site.

On the other hand, the electronic structure of K/Fe-SBA-15 interface is notably different than Fe-SBA-15 and Fe/Cu-SBA-15. The Fig. 5e, f shows that K atom sinks into the surface and interacts strongly with the hydroxyl groups of the surface. This effect drastically changes the electronic density of the active site. Moreover, it generates a site with depletion of the electronic density surrounding the K atom which can interact favorably with molecules with negative electronic density such as olefins. These results could be explained by the fact that potassium donates electrons to iron, facilitating CO chemisorption and dissociation, since CO tends to accept electrons from iron. Thus the addition of K promoter would facilitate CO chemisorption and olefins production. This result has been reported by other authors using other techniques [48].

Fig. 6 shows the projected density of states (p-DOS) of the different systems. In the case of SBA-15 (Fig. 6a) it can be seen the superposition of states at-2.5–6 eV, which indicates a covalent bond between silicon and oxygen atoms. The band gap energy is 3.8 eV, which indicates the insulator characteristic of this structure.

When an atom of iron is adsorbed on the surface (Fig. 6b) the interaction between Fe and OH groups mentioned above generates electronics sates close to the Fermi level, and this interaction provokes the decrease of band gap energy to 1.3 eV, generating a semiconductor interface.

In the case of the Fe/Cu-SBA-15 material (Fig. 6c), the electronic structures show the superposition of the electronic states between the Fe and Cu atoms at −1–3 eV. This would indicate the formation of a strong and stabilized bond forming a FeCu composites on the surface. This fact is consistent with the TEM micrographs that show bigger particles in the Fe/Cu-SBA-15 catalyst than in the other ones, and with the TPR profile where the signal around of 530 K was attributed to the likely reduction of $CuFeO_x$ to get CuFe species. The bond is formed from the 3d electronic states. In addition, Cu atoms generates states in the Fermi level, provoking a conduction of the electronic density in this bimetallic interface.

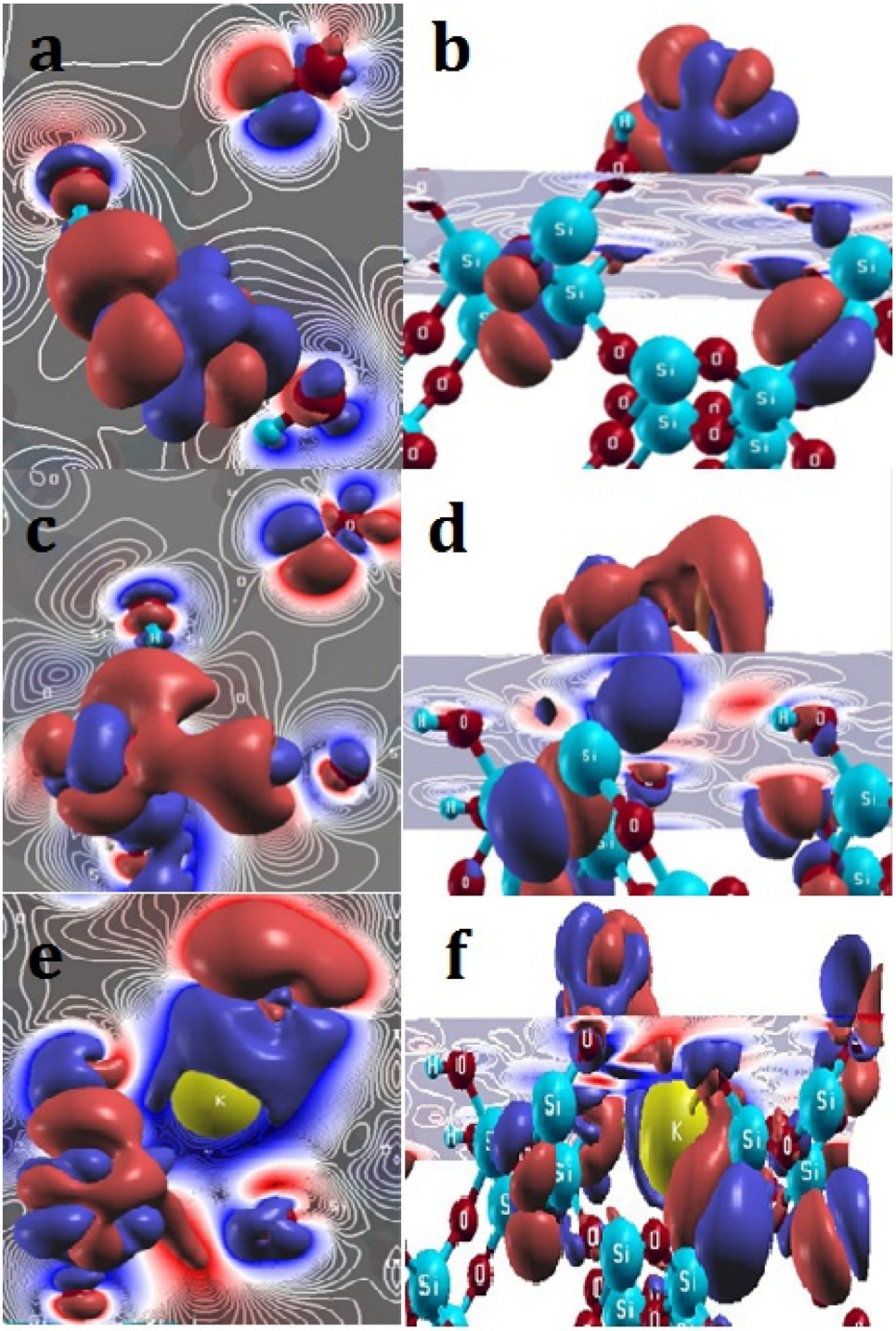


**Fig. 5.** Differential electronic density of catalysts.
a-b: Fe-SBA-15, c-d: Fe/Cu-SBA-15, e-f: Fe/K-SBA-15. Red lobules: accumulation of electronic density, blue lobules: depletion of electronic density. Value of isosurface: 0.001 ev/A3.

In the Fe/K-SBA15 interface, the p-DOS plot (Fig. 6d) indicates that the K atom does not present states under the Fermi level. In contrast to the FeCu case, the electronic states of iron are distributed in the valence band and in the Fermi level, creating a conductor interface.

In summary, DFT calculations indicate that the addition of K and Cu promoters in Fe-SBA15 surface, changes its electronic structure, creating conductor interfaces with different electronic density distribution, with depletion of electronic density on K atom, and accumulation of electronic density on the Cu atom. This distribution of electron density indicates that the presence of Cu generates an electronically different place because of the strong interaction between Fe-Cu, which could promote electronic restructuring of the active site as the FT reaction occurs, which would generate greater stability in catalyst activity over time.

In Fig. 7 are shown the results of the reaction tests for each catalyst. Fig. 7a, shows the conversion over time and it is shown that most of the catalysts reach a stationary state in the reaction time

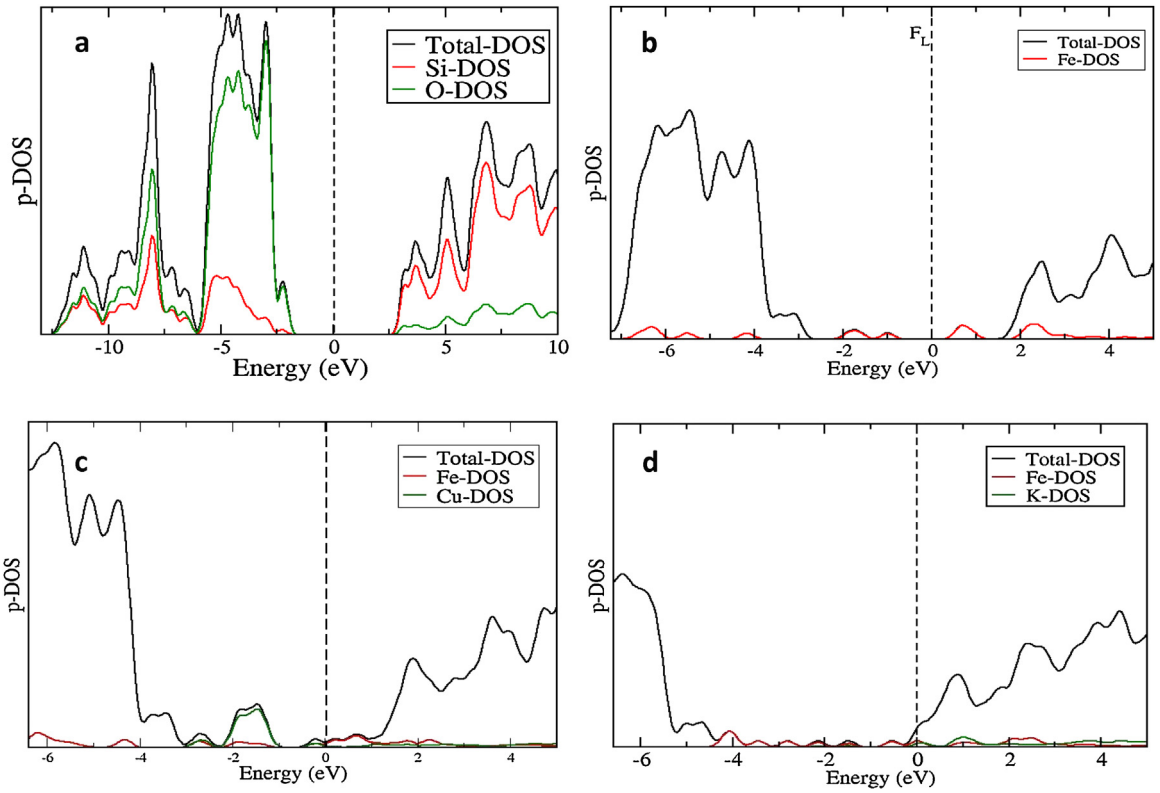


**Fig. 6.** Projected density of states (p-DOS) of the SBA-15 surface. a: clean, b: Fe-SBA15, c: Fe/Cu-SBA-15, d: Fe/K-SBA15.

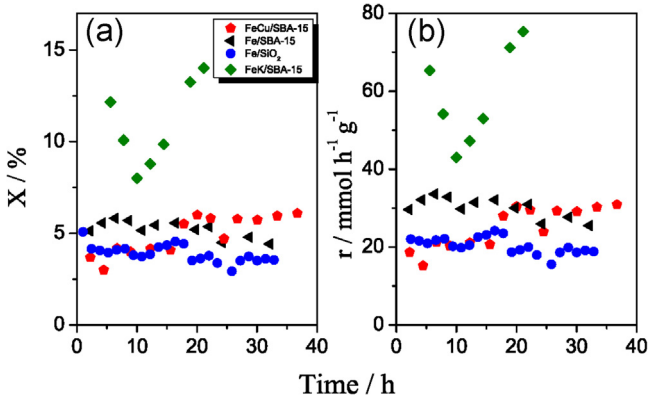


**Fig. 7.** Conversion and activity results of Fischer Tropsch reaction using the different catalysts.

studied, except the Fe/K-SBA-15 which shows a deactivation and a reactivation of the catalyst. This anomalous behavior has been previously reported for some iron catalysts in the FT reaction promoted with Ce, and could be attributed to reconstruction processes of the active phase [49].

In Fig. 7b is shown the intrinsic activity per gram of iron of the catalysts, in order to compare them independently of the metal loading. The results show clearly that the Fe/K-SBA-15 catalyst has the highest activity, showing the important role that the addition of K plays in the activity of Fe catalysts for FT synthesis. The comparison between Fe-$SiO_2$ and Fe-SBA-15 shows a higher activity in the latter, which could be attributed to the effect of using a mesoporous support with a high surface area, such as the SBA-15 which can stabilize nanoparticles of the active phase inside its pores, increasing the dispersion of the active phase. It is also observed that while Fe-SBA-15 has a tendency to decrease its activity with time, Fe/Cu-SBA-15 shows an opposite tendency, with a slight increase in its activity with time. This fact could be related to the effect of the addition of Cu, as we mentioned above from the TPR and DFT results, indicating that Cu addition on the Fe site generates a new active site, and the new electronic states formed could assist to the regeneration of the active site and this electronic effect can be stabilized the activity of the catalyst observed experimentally. According to some authors, the oxygen removal in the activation of catalysts (reduction whit $H_2$) is greatly promoted by introducing copper, because copper oxide can be easily reduced to its metallic state by reductants at low temperatures [50], and the metallic copper plays an essential role in helping the removal of oxygen atom from other oxide phases [51]. Furthermore, while the FT reaction occurs, metallic copper atoms, may weaken vicinal Fe–O bonds. This mechanism provides insight into enhancement of the carburization rate of FTS catalysts by copper promoter [52].

**Table 3**
Selectivity towards olefins.

| Catalyst | $C_2^=/C_2$ | $C_3^=/C_3$ | $C_2^=+C_3^=/C_2+C_3$ |
|---|---|---|---|
| *Fe-$SiO_2$* | 0.2 | 0.3 | 0.2 |
| *Fe-SBA-15* | 0.2 | 2.1 | 1.1 |
| *Fe/K-SBA-15* | 3.5 | 1.5 | 2.11 |
| *Fe/Cu-SBA-15* | 0.3 | 2.8 | 1.2 |

In Fig. 8 is shown the molar selectivity for each catalyst. In order to study them at similar conversions, data for the hydrocarbon production for the Fe/K-SBA-15 were taken at a conversion of 8% (at 10 h of reaction). The results show that Fe-$SiO_2$ presents the highest formation of $CH_4$ (that is undesirable), close to the 40%. In addition, the hydrocarbons formed grow up to $C_7$. By contrast, selectivity of Fe-SBA-15 shows minor formation of $CH_4$ and formation of hydrocarbons up to $C_{10}$. Table 3 shows the selectivity towards olefins ($C_2$ and $C_3$) of the catalysts, in those results it is also evident the highest selectivity of Fe-SBA-15 for the formation of these high-value

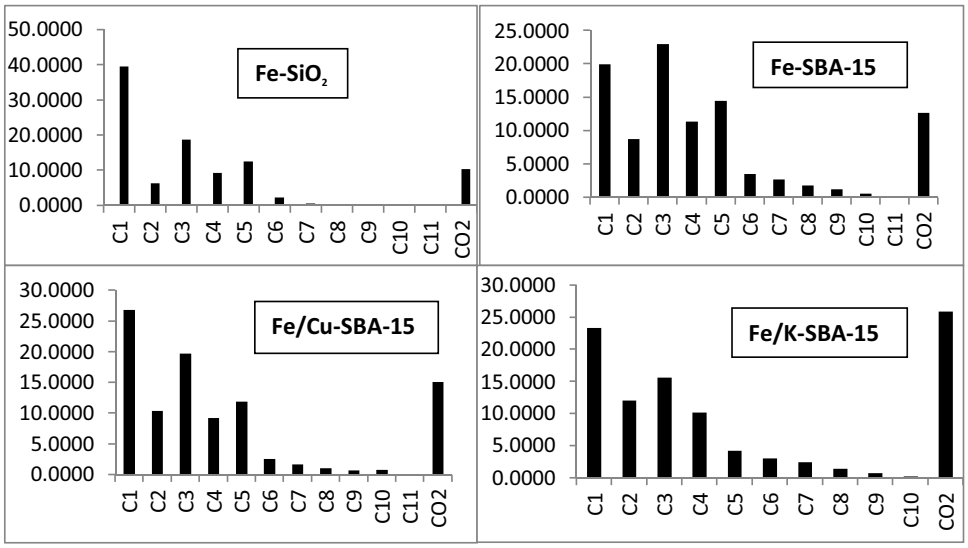


**Fig. 8.** Molar selectivity in FTS for each catalyst.

molecules compared to the Fe-$SiO_2$. This results show the beneficial role of using a porous $SiO_2$ support for Fe-supported catalysts, such as the SBA-15.

The selectivity of Fe/K-SBA-15 is similar to the one of Fe-SBA-15, but the main difference is in the highest formation of olefins observed in the former. As it was mentioned previously, the formation of this kind of molecules is highly desirable in FT catalysts. This behavior could be related to the electronic characteristics of the Fe/K-SBA-15 described in the DFT section, because the electronic density depletion created by the presence of K in the surface could stabilize molecules with high electron density such as olefins.

In the case of Fe/Cu-SBA-15, no major differences in selectivity are observed compared to Fe-SBA-15 sample.

## 4. Conclusions

Four different supported-iron catalysts were obtained and characterized. The characterization techniques showed that the ordered structure of the mesoporous material SBA-15 remained after the incorporation of the metals (Fe,Cu,K) and that they were incorporated within the channels of the SBA-15 support.

DFT calculations showed the exothermic energy of adsorption of Fe, FeCu and FeK over the simulated Surface of a SBA-15. In addition it was observed that the presence of K and Cu in the vicinity of Fe over the support surface creates new active sites, with the creation of conductor interfaces with different electronic density distribution. The FeCu system showed a great interaction between both metals, and accumulation of electronic density close to the copper atom. On the other hand, the presence of K creates sites with depletion on its electronic density close to the K atom and an electronic transfer towards the surface and the Fe atom.

The results of the catalytic tests performed showed firstly that the importance of porosity in silica supports for catalysts for the FT reaction, since Fe/SBA-15 showed a higher activity, major chain-growth formation of the products and more selectivity to olefins than the Fe/SiO2 catalyst.

Secondly, the effect of K and Cu as promoters showed that the addition of K enhances the catalytic activity and favors the selectivity to olefins. Both of these results are in agreement with the electronic properties of the surface described by the DFT calculations. On the other hand, the addition of Cu apparently increases the stability of the catalysts. As a result, the best performance in the FT reaction was obtained with FeCu/SBA-15 and FeK/SBA-15 catalysts, which add the positive effect of the metallic promoters to the positive effect of the porosity of the SBA-15.

## Acknowledgement

The authors acknowledge the financial support of ANPCyT (PICT-2011-2737), which allowed the development of this work.

## References

[1] M.E. Dry, Catal. Today 71 (2002) 227–241.
[2] M. Luo, H. Hamdeh, B.H. Davis, Catal. Today 140 (2009) 127–134.
[3] M. Luo, R.J. O'Brien, S. Bao, B.H. Davis, Appl. Catal. A: General 239 (2003) 111–120.
[4] G. Zhao, C. Zhang, S. Qin, H. Xiang, Y. Li, J. Mol. Catal. A: Chem. 286 (2008) 137–142.
[5] V.R.R. Pendyala, G. Jacobs, J.C. Mohandas, M. Luo, H.H. Hamdeh, Y. Ji, M.C. Ribeiro, B.H. Davis, Catal. Lett. 140 (2010) 98–105.
[6] S. Li, W. Ding, G.D. Meitzner, E. Iglesia, J. Phys. Chem. B 106 (2002) 85–91.
[7] T. Grzybek, J. Klinik, H. Papp, M. Baerns, Chem. Eng. Technol. 13 (1990) 156–161.
[8] S. Li, A. Li, S. Krishnamoorthy, E. Iglesia, Catal. Lett. 177 (2001) 197–205.
[9] S. Li, S. Krishnamoorthy, A. Li, G.D. Meitzner, E. Iglesia, J., Catal. 206 (2002) 202–217.
[10] Y. Jin, A.K. Datye, J. Catal. 196 (2000) 8–17.
[11] R.J. O'Brien, L. Xu, R.L. Spicer, S. Bao, D.R. Milburn, B.H. Davis, Catal. Today 36 (1997) 325–334.
[12] I.E. Wachs, D.J. Duyer, E. Iglesia, Appl. Catal. 12 (1984) 201–217.
[13] D.B. Bukur, D. Mukesh, S.A. Patel, Ind. Eng. Chem. Res. 29 (1990) 194–204.
[14] A.F.H. Wielers, G.W. Koebrugge, J.W. Geus, J., Catal. 121 (1990) 375–385.
[15] A.F.H. Wielers, C.E.C.A. Hop, J. van Beijnum, A.M. van der Kraan, J.W. Geus, J. Catal. 121 (1990) 364–374.
[16] E. de Smit, A.W. Beale, S. Nikitenko, B.M. Weckhuysen, J. Catal. 262 (2009) 244–256.
[17] M. Boudart, A. Delbouille, J.A. Dumesic, S. Khammouma, H. Topsøe, J. Catal. 37 (1975) 486–502.
[18] M.A. McDonald, D.A. Storm, M. Boudart, J. Catal. 102 (1986) 386–400.
[19] E.I. Mabaso, E. van Steen, M. Claeys, DGMK Tagungsbericht 4 (2006) 93–100.
[20] L.A. Cano, M.V. Cagnoli, N.A. Fellenz, J.F. Bengoa, N.G. Gallegos, A.M. Alvarez, S.G. Marchetti, Appl. Catal. A 379 (2010) 105–110.
[21] P.B. Radstake, J.P. den Breejen, G.L. Bezemer, J.H. Bitter, K.P. de Jong, V. Frøseth, A. Holmen, Stud. Surf. Sci. Catal. 167 (2007) 85–90.
[22] G.L. Bezemer, J.H. Bitter, H.P.C.E. Kuipers, H. Oosterbeek, J.E. Holewijn, X. Xu, F. Kapteijn, A.J. van Dillen, K.P. de Jong, J. Am. Chem. Soc. 128 (2006) 3956–3964.
[23] D. Zhao, J. Feng, Q. Huo, N. Melosh, G.H. Fredrickson, B.F. Chmelka, G.D. Stucky, Science 279 (1998) 548–552.
[24] D. Zhao, Q. Huo, J. Feng, B.F. Chmelka, G.D. Stucky, J. Am. Chem. Soc. 120 (1998).
[25] J.C. Park, S.C. Yeo, D.H. Chun, J.T. Lim, J. Yang, H. Lee, S. Hong, H.M. Lee, C.S. Kimc, H. Jung, J. Mater. Chem. A. 35 (2014) 1–9.
[26] M.E. Dry, Stud. Surf. Sci. Catal. 152 (2004) 533–600.
[27] J. Villarroel-Rocha, D. Barrera, K. Sapag, Micropor. Mesopor. Mat. 200 (2014) 68–78.

[28] J. Perdew, K. Burke, M. Ernzerhof, Phys. Rev. Lett. 77 (1996) 3865–3868.
[29] M. Soler, E. Artacho, J.D. Gale, A. Garc, J. Junquera, P. Ordej, S. Daniel, Journal. Phys. Condens. Matter. 14 (2002) 2745–2779.
[30] N. Troullier, J.L. Martins, Phys. Rev. B 43 (1991) 8861–8869.
[31] W.W. Schmahl, I.P. Swainson, M.T. Dove, A. Graeme-Barber, Z. Kristallographie 201 (1992) 125–145.
[32] A.S.M. Chong, X.S. Zhao, J. Phys. Chem. B 107 (2003) 12650–12657.
[33] A. Kokalj, A. Dal Corso, S. de Gironcoli, S. Baroni, J. Phys. Chem. B 106 (2002) 9839–9846.
[34] A. Kokalj, Comput. Mater. Sci. 28 (2003) 155–168.
[35] J.R.A. Sietsma, J.P. den Breejen, P.E. de Jongh, A.J. van Dillen, J.H. Bitter, K.P. de Jong, Stud. Surf. Sci. Catal. 167 (2007) 55–60.
[36] J.P. den Breejen, J.R.A. Sietsma, H. Friedrich, J.H. Bitter, K.P. de Jong, J. Catal. 270 (2010) 146–152.
[37] X. Wang, Q. Zhang, S. Yang, Y. Wang, J. Phys. Chem. B 109 (2005) 23500–235008.
[38] A.V. Neimark, P.I. Ravikovitch, Micropor. Mesopor. Mat. 44 (2001) 697–707.
[39] M. Thommes, Chem. Ing. Tech. 82 (2010) 1059–1073.
[40] M. Thommes, K. Kaneko, A.V. Neimark, J.P. Olivier, F. Rodríguez-Reinoso, J. Rouquerol, K.S. Sing, Pure Appl. Chem. 87 (2015) 1051–1069.
[41] P. Van der Voort, P.I. Ravikovitch, K.P. de Jong, M. Benjelloun, E. Van Bavel, A.H. Janssen, A.V. Neimark, B.M. Weckhuysen, E.F. Vansant, J. Phys. Chem. B 106 (2002) 5873–5877.
[42] P. Van der Voort, P.I. Ravikovitch, K.P. De Jong, A.V. Neimark, A.H. Janssen, M. Benjelloun, E. Van Bavel, P. Cool, B.M. Weckhuysen, E.F. Vansant, Chem. Commun (2002) 1010–1011.
[43] V. Meynen, P. Cool, E.F. Vansant, Micropor. Mesopor. Mat. 104 (2007) 26–38.
[44] L.A. Cano, J.F. Bengoa, S.J. Stewart, R.C. Mercader, S.G. Marchetti, Hyperfine Interact. 195 (2010) 93–98.
[45] S. Yang, W. Zhu, Q. Zhang, Y. Wang, J. Catal. 254 (2008) 251–262.
[46] H. Chu, L. Yang, Q. Zhang, Y. Wang, J. Catal. 241 (2006) 225–228.
[47] D. Zhou, B. Li, Z. Ma, X. Huang, X. Zhang, H. Yang, J. Mol. Catal. A: Chem. 409 (2015) 183–190.
[48] H. Wan, B. Wu, C. Zhang, H. Xiang, Y. Li, J. Mol. Catal. A: Chem. 283 (2008) 33–42.
[49] T. Herranz, S. Rojas, F.J. Pérez-Alonso, M. Ojeda, P. Terreros, J.L. García Fierro, J. Catal. 243 (2006) 199–211.
[50] Y. Jin, A.K. Datye, J. Catal. 196 (2000) 8–17.
[51] D.B. Bukur, K. Okabe, M.P. Rosynek, C. Li, D. Wang, K.R.P.M. Rao, G.P. Huffman, J. Catal. 155 (1995) 353–365.
[52] C.H. Zhang, Y. Yang, B.T. Teng, T.Z. Li, J. Catal. 237 (2006) 405–415.